Volume 56
Number 38
11 May 2020
Pages 5069–5196

ChemComm

Chemical Communications

rsc.li/chemcomm

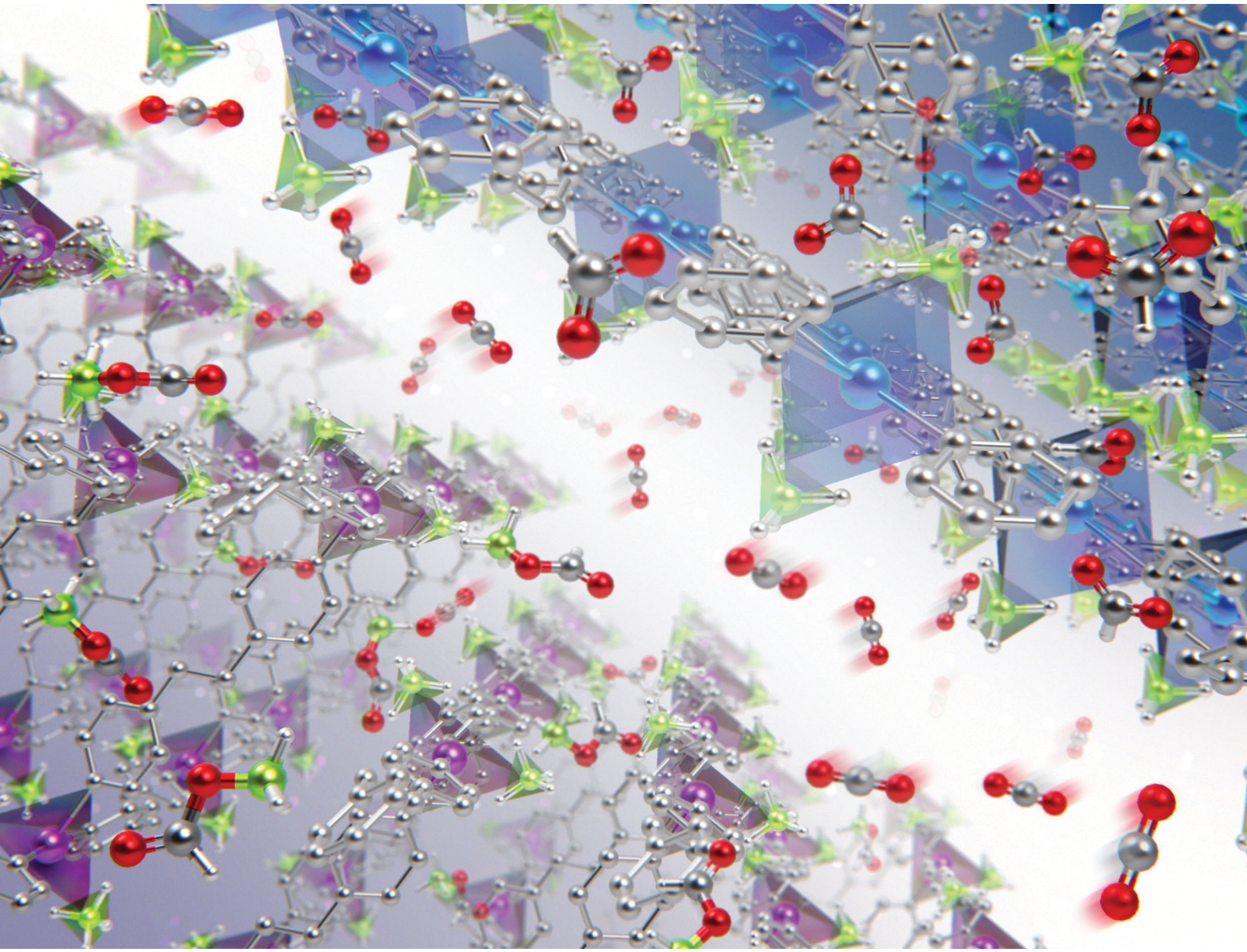

ISSN 1359-7345

ROYAL SOCIETY OF CHEMISTRY

COMMUNICATION

Satoshi Horike *et al.*

Reactivity of borohydride incorporated in coordination polymers toward carbon dioxide

ChemComm

COMMUNICATION

View Article Online
View Journal | View Issue

Cite this: *Chem. Commun.*, 2020, **56**, 5111

Received 6th March 2020,
Accepted 6th April 2020

DOI: 10.1039/d0cc01753a

rsc.li/chemcomm

Reactivity of borohydride incorporated in coordination polymers toward carbon dioxide†

Kentaro Kadota, [a] Easan Sivaniah [ab] and Satoshi Horike *[bcde]

Borohydride (BH_4^-)-containing coordination polymers converted CO_2 into HCO_2^- or $[BH_3(OCHO)]^-$, whose reaction routes were affected by the electronegativity of metal ions and the coordination mode of BH_4^-. The reactions were investigated using thermal gravimetric analysis under CO_2 gas flow, infrared spectroscopy, and NMR experiments.

Conversion of carbon dioxide (CO_2) into valuable chemicals is a key to realize a sustainable society.[1,2] In particular, it is essential to establish chemical reactions that transform CO_2 into various types of chemical moieties under mild conditions.[3] However, the inherent inertness of CO_2 has hampered the utilization of CO_2 in transformation reactions. To overcome the inertness, various catalytic and stoichiometric reactions have been widely studied in both solution and the solid-state, including metals, metal oxides,[4] metal complexes,[5,6] and metal-free organic molecules.[7]

Borohydride (BH_4^-), a hydride-based complex anion, has been commonly utilized as a reducing agent. In the solution phase, metal borohydrides (MBHs) stoichiometrically react with CO_2 at ambient temperatures and pressures.[8–11] BH_4^- in solution is able to convert CO_2 into chemical species such as formate (HCO_2^-) and formylhydroborate ($[BH_{4-x}(OCHO)_x]^-$, $x = 1$, 2 and 3) depending on the reaction conditions, *e.g.* counter cations, temperatures, solvents, and pressures.[8,9,12] The solid-state reactivity of BH_4^- toward CO_2 is also interesting from the viewpoint of heterogeneous catalysts and CO_2 scrubbers. Nevertheless, limited studies have been performed on the solid-state reactivity of MBHs toward CO_2.[13,14] This is because slow diffusion of CO_2 in dense MBHs results in low reactivity under mild conditions.[14] Although porous structures are advantageous for the diffusion of CO_2, MBHs with the porous structure are limited except for a few examples, *e.g.* γ-$Mg(BH_4)_2$.[14,15]

Coordination polymers (CPs) and metal–organic frameworks (MOFs) are crystalline solids constructed from metal ions and bridging organic linkers.[16–18] Their open structures have offered an attractive platform for various gas–solid reactions, such as CO_2 sorption[19–21] and post-synthetic modification.[22,23] In addition, rich structural and chemical tunability of CPs demonstrated the controlled reactivity of reactive species, *e.g.* radicals,[24,25] imines,[26] and photoactive metal complexes.[27] CPs are a promising platform for solid–gas reactions between BH_4^- and CO_2. BH_4^--containing CPs are constructed from metal ions (*e.g.* Mg^{2+}, Ca^{2+}, Mn^{2+}, Zn^{2+}, and Th^{4+}) and N-based neutral linkers show various types of the chemical environment of BH_4^-.[28–30] Here, we investigate the reactivity of BH_4^--containing CPs to convert CO_2 into HCO_2^- or $[BH_3(OCHO)]^-$ under mild conditions depending on their structures.

$[M(BH_4)_2(pyz)_2]$ (**M-pyz**, M = Mg^{2+}, Ca^{2+}, pyz = pyrazine)[28,29] were selected to investigate the influence of metal ions on the reactivity of BH_4^- toward CO_2. The metal ion center shows an octahedral geometry and the two BH_4^- ions coordinate in the axial positions (Fig. 1A). The extended structure of **M-pyz** comprises a 2D square grid constructed by $[M_4pyz_4]$ units (Fig. 1B). The electronic properties and reactivity of BH_4^- are influenced by the electronegativity of counter metal ions.[31,32] Attempts at the synthesis of isostructural **M-pyz** were made using a Mn^{2+}-based MBH precursor. $[Mn(BH_4)_2{\cdot}3THF]{\cdot}NaBH_4$ was prepared following the literature methods.[33] The general synthetic method involves mechanochemical milling of the MBH precursor and pyz under Ar. **Mg-pyz** was previously

[a] *Department of Molecular Engineering, Graduate School of Engineering, Kyoto University, Katsura, Nishikyo-ku, Kyoto 615-8510, Japan*
[b] *Institute for Integrated Cell-Material Sciences, Institute for Advanced Study, Kyoto University, Yoshida, Sakyo-ku, Kyoto 606-8501, Japan. E-mail: horike@icems.kyoto-u.ac.jp*
[c] *AIST-Kyoto University Chemical Energy Materials Open Innovation Laboratory (ChEM-OIL), National Institute of Advanced Industrial Science and Technology (AIST), Yoshida-Honmachi, Sakyo-ku, Kyoto 606-8501, Japan*
[d] *Department of Synthetic Chemistry and Biological Chemistry, Graduate School of Engineering, Kyoto University, Katsura, Nishikyo-ku, Kyoto 615-8510, Japan*
[e] *Department of Materials Science and Engineering, School of Molecular Science and Engineering, Vidyasirimedhi Institute of Science and Technology, Rayong 21210, Thailand*

† Electronic supplementary information (ESI) available. See DOI: 10.1039/d0cc01753a

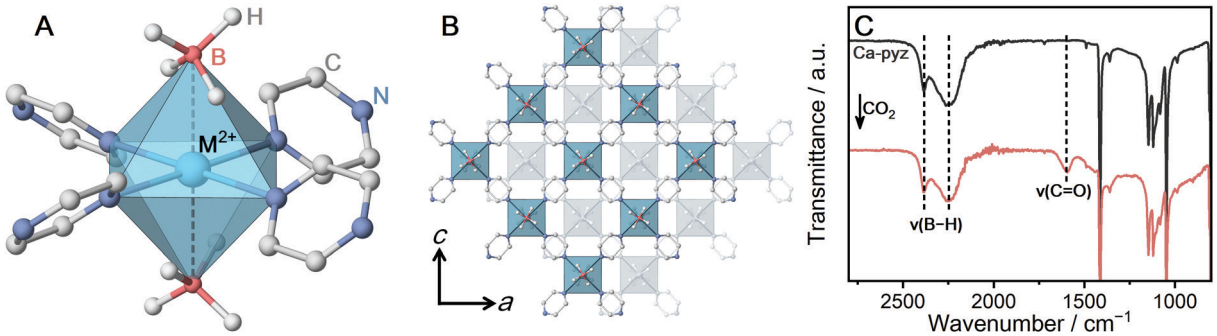

Fig. 1 (A) Local coordination geometry of **M-pyz** (M = Mg^{2+}, Ca^{2+}, Mn^{2+}). (B) ABAB stacking structure of the extended 2D layers of **M-pyz** (M = Mg^{2+}, Ca^{2+}, Mn^{2+}). (C) IR spectra of **Ca-pyz** before and after CO_2 adsorption at 25 °C.

synthesized in the solution phase, whereas the solvent-free conditions afford a highly crystalline product as well (Fig. S1, ESI†). The powder X-ray diffraction (PXRD) pattern of **Mn-pyz** shows a good agreement with that of **Mg-pyz** (Fig. S1, ESI†).

The solid-state synthesis of **M-pyz** proceeds without solvents at 25 °C within 30 min. The fast reaction kinetics in the solid-state is ascribed to the low melting point of pyz (52 °C). The lower melting point of reactants leads to higher molecular mobility, enhancing the reactivity in the solid-state.[34] Mechanical milling is useful to synthesize CPs from MBHs because most of the MBHs are poorly soluble in common organic solvents. The thermal properties were characterized by thermal gravimetric analysis (TGA) under N_2 (Fig. S2, ESI†). Each compound exhibits a weight loss at relatively low temperatures; 50, 70, and 70 °C for **Mg-**, **Mn-**, and **Ca-pyz** due to the low boiling point of pyz (115 °C). Isothermal TGA measurements at 40 °C under N_2 indicate that **Ca-pyz** shows higher thermal stability than **Mn-pyz** (weight loss after 6 hours; 0.2 *vs.* 3.2 wt%, Fig. S3, ESI†). In the case of MBHs, electropositive metal ions construct MBHs with higher thermal stability.[35] Meanwhile, in the case of BH_4^--containing CPs, the strength of the coordination bonds is also essential. The Hard and Soft Acids and Bases (HSAB) theory reveals that electropositive metal ions (hard acids) form weaker coordination bonds with nitrogen-based linkers (soft bases) such as pyz. Therefore, the trend of thermal stability for **M-pyz** does not simply follow the electronegativity of metal ions (thermal stability: Mg < Mn < Ca, Pauling electronegativity: Ca < Mg < Mn).

To characterize the chemical environment of BH_4^- in the CP, solid-state ^{11}B magic angle spinning (MAS) nuclear magnetic resonance (NMR) was carried out on non-paramagnetic **Ca-pyz**. The ^{11}B NMR spectrum of **Ca-pyz** displays a peak at −36 ppm corresponding to the signal of BH_4^- (Fig. S4, ESI†). The total charge on BH_4^- is correlated with the chemical shift of ^{11}B NMR: electron-rich BH_4^- shows a peak in a lower frequency.[31] The low-frequency shift of the ^{11}B peak indicates that BH_4^- in **Ca-pyz** is more electron-rich than $Ca(BH_4)_2$. In the framework of **Ca-pyz**, the Lewis acidity of Ca^{2+} was reduced by electron donation from the coordinating pyz molecules, which leads to the formation of electron-rich BH_4^-.[29]

CO_2 adsorption measurement was carried out to evaluate the reactivity of **Ca-pyz** in gas–solid equilibrium. The CO_2 isotherm at 25 °C displays irreversible adsorption (7 mL g^{-1} at 100 kPa), which is characteristic of chemisorption behavior (Fig. S5, ESI†).[36] The IR spectrum of **Ca-pyz** after CO_2 adsorption displays a new peak at 1600 cm^{-1}, corresponding to C=O stretching (Fig. 1C). The solid-state ^1H–^{13}C cross-polarization (CP) MAS NMR spectrum of **Ca-pyz** after CO_2 adsorption shows peaks at 170 and 145 ppm. The peaks correspond to the signals of HCO_2^- and pyz, respectively (Fig. S6, ESI†). The results indicate that BH_4^- in **Ca-pyz** reduces CO_2 to HCO_2^- with the release of diborane (B_2H_6) as a by-product.[10]

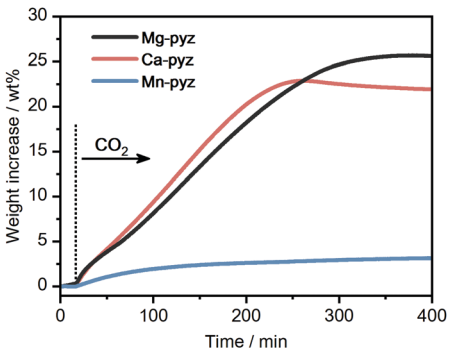

Fig. 2 Isothermal TGA profiles of **M-pyz** (M = Mg^{2+}, Ca^{2+}, Mn^{2+}) under CO_2 flow (0.1 MPa, 30 mL min^{-1}) at 40 °C.

The kinetic reactivity of **M-pyz** toward CO_2 was evaluated using isothermal TGA under CO_2 flow. Fig. 2 displays the TGA profiles of each powder sample (10 mg) under CO_2 flow (0.1 MPa, 30 mL min^{-1}) at 40 °C. **Mg-pyz** and **Ca-pyz** exhibit higher weight increases than **Mn-pyz** (25.5, 21.9, and 3.2 wt% after 400 min, respectively). **Ca-pyz** was amorphous after the CO_2 reaction, as confirmed by PXRD (Fig. S7, ESI†). To identify the chemical species after the CO_2 reaction, solution NMR was carried out on **Ca-pyz** dissolved in DMSO-d_6. The solution ^{13}C NMR spectrum of **Ca-pyz** after the CO_2 reaction displays peaks at 167, 146, 53, 50, 47 and 44 ppm (Fig. S8, ESI†). The peaks at 167 and 146 ppm correspond to the ^{13}C signals of HCO_2^- and pyz, respectively. The peak at 47 ppm is assigned to piperazine formed by the reduction of pyz by B_2H_6, whereas the rest of the peaks are not able to be assigned.[29,37] The higher reactivity of **Ca-pyz** toward CO_2 is attributed to the preferable electronic

interaction between Ca^{2+} (hard acid) and HCO_2^- (hard base) rather than BH_4^- (soft base).

The formation of $[BH_{4-x}(OCHO)_x]^-$ from BH_4^- and CO_2 was investigated at a BH_4^--containing CP. Given that $[BH_{4-x}(OCHO)_x]^-$ is bulky than HCO_2^-, $[Mn(BH_4)_2(dpe)_{1.5}]$ (**Mn-dpe**, dpe = dipyridylethane) having voids was selected.[28] The two BH_4^- ions coordinate to the Mn^{2+} center in a bidentate manner, which was confirmed by single-crystal X-ray diffraction (SC-XRD) in Fig. 3A. The extended structure of **Mn-dpe** comprises a 1D ladder constructed from [Mn4dpe4] units (Fig. 3B). The coordination mode of BH_4^- was confirmed by IR spectroscopy as well. The IR spectrum of **Mn-dpe** displays two stretching peaks in the B–H stretching region at 2378 and 2127 cm^{-1}, respectively (Fig. 4B). The peak at 2378 cm^{-1} corresponds to the B–H bond coordinating to the Mn^{2+} center, whereas the peak at 2127 cm^{-1} corresponds to the non-coordinating B–H.[38] In contrast to the broadened B–H stretching peak of **Ca-pyz** (Fig. 1C), **Mn-dpe** displays distinct two peaks of B–H stretching, which is originated from a stronger binding interaction between Mn^{2+} (soft acid) and BH_4^- (soft base).

The kinetic curve of the CO_2 reaction with **Mn-dpe** was collected using the same procedure as **M-pyz** (Fig. 3B). **Mn-dpe** demonstrates a weight increase of 26.2 wt% after 600 min at 40 °C, which corresponds to a value of the 1.1 : 1 molar ratio of reacted CO_2 per BH_4^-. After the CO_2 reaction, **Mn-dpe** shows small diffraction peaks different from the original peaks (Fig. S9, ESI†). Solution ^{11}B NMR measurement was carried out to determine the chemical species after the CO_2 reaction. The $^{11}B\{^1H\}$ NMR spectrum of digested **Mn-dpe** after the CO_2 reaction displays the peaks at −33, −11, and 2.2 ppm in Fig. 4A. The broad peaks were observed due to the paramagnetic effect of Mn^{2+}. The ^{11}B peaks correspond to BH_4^-, $[BH_3(OCHO)]^-$ and $[BH_2(OCHO)_2]^-$, respectively.[9,39] Successive CO_2 insertions into the B–H bond of BH_4^- produce $[BH_{4-x}(OCHO)_x]^-$, and the number of reacted CO_2 molecules is affected by the reaction conditions such as pressure and temperature in the solution phase.[8,9] The reaction of $NaBH_4$ in acetonitrile with 0.1 MPa of CO_2 for 10 minutes produces $[BH(OCHO)_3]^-$ as a major product, and $[BH_3(OCHO)]^-$ is not observed.[9] This is because all the hydrogen atoms of BH_4^- dissociated in acetonitrile are available for the reaction with CO_2. On the other hand, in the case of **Mn-dpe**, two of the hydrogen atoms of BH_4^- are pinned with the Mn^{2+} center by a coordination bond as confirmed by SC-XRD and IR spectroscopy. After the CO_2 reaction, a non-coordinating B–H stretching peak was not observed, and this is because of the reaction with CO_2 to form $[BH_3(OCHO)]^-$ and $[BH_2(OCHO)_2]^-$ in Fig. 4B. The coordinating B–H stretching peak is preserved after the CO_2 reaction, indicating the coordinating bonds between Mn^{2+} and $[BH_3(OCHO)]^-$ or $[BH_2(OCHO)_2]^-$. A sluggish kinetics of dense $NaBH_4$ in the solid-state toward CO_2 indicates that the open structure of **Mn-dpe** is essential for the diffusion of CO_2 (Fig. 3C). Based on the results, the reaction between **Mn-dpe** and CO_2 to produce $[BH_3(OCHO)]^-$ and $[BH_2(OCHO)_2]^-$ is proposed (Fig. S11, ESI†). The results indicate that the anisotropic coordination geometry of BH_4^- in **Mn-dpe** affects the reaction route with CO_2.

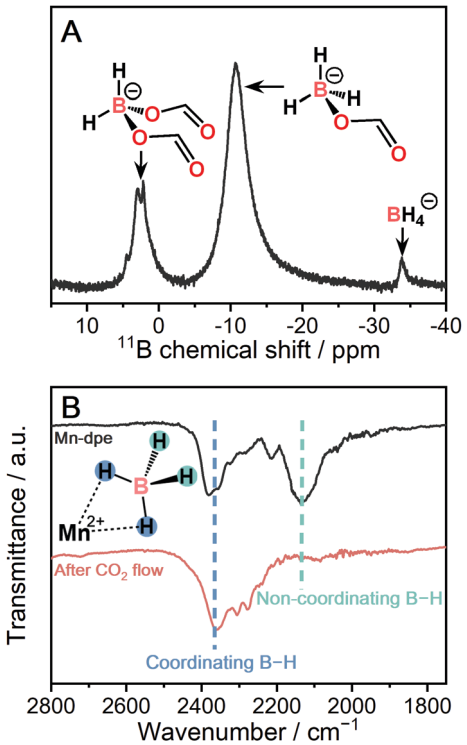

Fig. 4 (A) Solution $^{11}B\{^1H\}$ NMR of digested **Mn-dpe** after CO_2 reaction. (B) IR spectra of **Mn-dpe** before and after the CO_2 reaction.

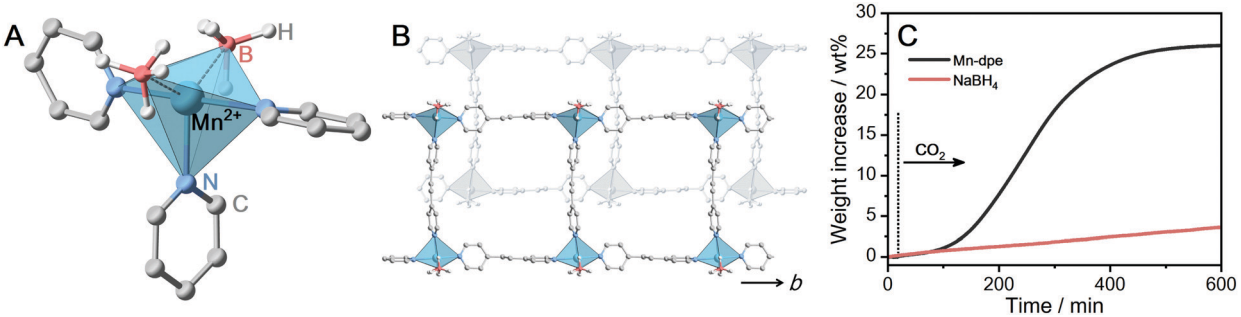

Fig. 3 (A) Local coordination geometry of **Mn-dpe**. (B) Packing structure of the extended 1D ladders of **Mn-dpe**. (C) Isothermal TGA profiles of **Mn-dpe** and $NaBH_4$ under CO_2 flow (0.1 MPa, 30 mL min^{-1}) at 40 °C.

In conclusion, we demonstrated the reactivity of BH_4^- toward CO_2 which is correlated with the crystal structures of BH_4^--containing coordination polymers. The reactivity of $[M(BH_4)_2(pyrazine)_2]$ (M = Mg^{2+}, Mn^{2+}, Ca^{2+}) and $[Mn(BH_4)_2(dipyridylethane)_{1.5}]$ toward CO_2 at 40 °C was investigated by using isothermal TGA under CO_2 flow, IR and NMR. BH_4^- in $[Ca(BH_4)_2(pyrazine)_2]$ converted CO_2 into HCO_2^-. The BH_4^- pinned by coordination bonds with Mn^{2+} in $[Mn(BH_4)_2(dipyridylethane)_{1.5}]$ regulated the successive CO_2 insertion reaction and produced $[BH_3(OCHO)]^-$ as a major species. The structural diversity of coordination polymers provides a new approach to regulate the reaction routes between BH_4^- and CO_2 in the solid-state.

The work was supported by the Japan Society of the Promotion of Science (JSPS) for a Grant-in-Aid for Scientific Research (B) (JP18H02032), the Challenging Research (Exploratory) (JP19K22200) from the Ministry of Education, Culture, Sports, Science and Technology, Japan, and Strategic International Collaborative Research Program (SICORP), the Adaptable and Seamless Technology Transfer Program through Target-driven R&D (A-STEP) from the Japan Science and Technology, Japan, Inamori Research Grants, and Tokuyama Science Foundation.

Conflicts of interest

The authors declare no conflict of interest.

References

1 T. Sakakura, J.-C. Choi and H. Yasuda, *Chem. Rev.*, 2007, **107**, 2365–2387.
2 J. Artz, T. E. Muller, K. Thenert, J. Kleinekorte, R. Meys, A. Sternberg, A. Bardow and W. Leitner, *Chem. Rev.*, 2018, **118**, 434–504.
3 Q. Liu, L. Wu, R. Jackstell and M. Beller, *Nat. Commun.*, 2015, **6**, 5933.
4 J. L. White, M. F. Baruch, J. E. P. Iii, Y. Hu, I. C. Fortmeyer, J. E. Park, T. Zhang, K. Liao, J. Gu, Y. Yan, T. W. Shaw, E. Abelev and A. B. Bocarsly, *Chem. Rev.*, 2015, **115**, 12888–12935.
5 A. J. Morris, G. J. Meyer and E. Fujita, *Acc. Chem. Res.*, 2009, **42**, 1983–1994.
6 B. J. Cook, G. N. Di Francesco, K. A. Abboud and L. J. Murray, *J. Am. Chem. Soc.*, 2018, **140**, 5696–5700.
7 D. W. Stephan and G. Erker, *Angew. Chem., Int. Ed.*, 2015, **54**, 6400–6441.
8 G. La Monica, G. A. Ardizzoia, F. Cariati, S. Cenini and M. Pizzotti, *Inorg. Chem.*, 1985, **24**, 3920–3923.
9 I. Knopf and C. C. Cummins, *Organometallics*, 2015, **34**, 1601–1603.
10 S. Murugesan, B. Stöger, M. Weil, L. F. Veiros and K. Kirchner, *Organometallics*, 2015, **34**, 1364–1372.
11 J. G. Burr, W. G. Brown and H. E. Heller, *J. Am. Chem. Soc.*, 1950, **72**, 2560–2562.
12 K. Kadota, N. T. Duong, Y. Nishiyama, E. Sivaniah and S. Horike, *Chem. Commun.*, 2019, **55**, 9283–9286.
13 J. Zhang and J. W. Lee, *Carbon*, 2013, **53**, 216–221.
14 J. G. Vitillo, E. Groppo, E. G. Bardaji, M. Baricco and S. Bordiga, *Phys. Chem. Chem. Phys.*, 2014, **16**, 22482–22486.
15 Y. Filinchuk, B. Richter, T. R. Jensen, V. Dmitriev, D. Chernyshov and H. Hagemann, *Angew. Chem., Int. Ed.*, 2011, **50**, 11162–11166.
16 S. Kitagawa, R. Kitaura and S. Noro, *Angew. Chem., Int. Ed.*, 2004, **43**, 2334–2375.
17 O. M. Yaghi, M. O'Keeffe, N. W. Ockwig, H. K. Chae, M. Eddaoudi and J. Kim, *Nature*, 2003, **423**, 705–714.
18 G. Férey, *Chem. Soc. Rev.*, 2008, **37**, 191–214.
19 T. M. McDonald, J. A. Mason, X. Kong, E. D. Bloch, D. Gygi, A. Dani, V. Crocella, F. Giordanino, S. O. Odoh, W. S. Drisdell, B. Vlaisavljevich, A. L. Dzubak, R. Poloni, S. K. Schnell, N. Planas, K. Lee, T. Pascal, L. F. Wan, D. Prendergast, J. B. Neaton, B. Smit, J. B. Kortright, L. Gagliardi, S. Bordiga, J. A. Reimer and J. R. Long, *Nature*, 2015, **519**, 303–308.
20 A. Phan, C. J. Doonan, F. J. Uribe-Romo, C. B. Knobler, M. O'Keeffe and O. M. Yaghi, *Acc. Chem. Res.*, 2010, **43**, 58–67.
21 E. González-Zamora and I. A. Ibarra, *Mater. Chem. Front.*, 2017, **1**, 1471–1484.
22 M. Servalli, M. Ranocchiari and J. A. Van Bokhoven, *Chem. Commun.*, 2012, **48**, 1904–1906.
23 V. Guillerm, H. Xu, J. Albalad, I. Imaz and D. Maspoch, *J. Am. Chem. Soc.*, 2018, **140**, 15022–15030.
24 H. Sato, R. Matsuda, K. Sugimoto, M. Takata and S. Kitagawa, *Nat. Mater.*, 2010, **9**, 661–666.
25 T. B. Faust and D. M. D'Alessandro, *RSC Adv.*, 2014, **4**, 17498–17512.
26 T. Haneda, M. Kawano, T. Kawamichi and M. Fujita, *J. Am. Chem. Soc.*, 2008, **130**, 1578–1579.
27 S. S. Kaye and J. R. Long, *J. Am. Chem. Soc.*, 2008, **130**, 806–807.
28 K. Kadota, N. T. Duong, Y. Nishiyama, E. Sivaniah, S. Kitagawa and S. Horike, *Chem. Sci.*, 2019, **10**, 6193–6198.
29 M. J. Ingleson, J. P. Barrio, J. Bacsa, A. Steiner, G. R. Darling, J. T. A. Jones, Y. Z. Khimyak and M. J. Rosseinsky, *Angew. Chem., Int. Ed.*, 2009, **48**, 2012–2016.
30 J. McKinven, G. S. Nichol and P. L. Arnold, *Dalton Trans.*, 2014, **43**, 17416–17421.
31 Z. Łodziana, P. Błoński, Y. Yan, D. Rentsch and A. Remhof, *J. Phys. Chem. C*, 2014, **118**, 6594–6603.
32 Y. Nakamori, H. Li, K. Miwa, S.-I. Towata and S.-I. Orimo, *Mater. Trans.*, 2006, **47**, 1898–1901.
33 V. D. Makhaev, A. P. Borisov, T. P. Gnilomedova, É. B. Lobkovskii and A. N. Chekhlov, *Bull. Acad. Sci. USSR, Div. Chem. Sci.*, 1987, **36**, 1582–1586.
34 A. Pichon and S. L. James, *CrystEngComm*, 2008, **10**, 1839–1847.
35 Y. Nakamori, K. Miwa, A. Ninomiya, H. Li, N. Ohba, S. Towata, A. Züttel and S. Orimo, *Phys. Rev. B: Condens. Matter Mater. Phys.*, 2006, **74**, 045126.
36 J. G. Bell, S. A. Morris, F. Aidoudi, L. J. McCormick, R. E. Morris and K. M. Thomas, *J. Mater. Chem. A*, 2017, **5**, 23577–23591.
37 B. Chatterjee and C. Gunanathan, *J. Chem. Sci.*, 2019, **131**, 118.
38 T. J. Marks and J. R. Kolb, *Chem. Rev.*, 1977, **77**, 263–293.
39 C. V. Picasso, D. A. Safin, I. Dovgaliuk, F. Devred, D. Debecker, H.-W. Li, J. Proost and Y. Filinchuk, *Int. J. Hydrogen Energy*, 2016, **41**, 14377–14386.

